Growth and fluctuations of suncups on alpine snowpacks

Kevin A. Mitchell[1] and T. Tiedje[2]

Received 23 March 2010; revised 15 August 2010; accepted 13 September 2010; published 21 December 2010.

[1] A mathematical model for suncups on glacier and alpine snow during the summer melting season is compared with time-lapse field observations. The model consists of a nonlinear partial differential equation whose solution spontaneously forms quasi-periodic patterns similar to suncups when started from a random initial condition. The suncup patterns are found to fully develop in 5 days in the field under full sun. The patterns fluctuate chaotically in time, both in the observations and in the model. The fluctuations can be described mathematically in terms of diffusion of individual suncups. According to the model, the rate at which the suncups diffuse contains information about the effect of the suncups on the albedo of the snow.

Citation: Mitchell, K. A., and T. Tiedje (2010), Growth and fluctuations of suncups on alpine snowpacks, *J. Geophys. Res.*, *115*, F04039, doi:10.1029/2010JF001724.

1. Introduction

[2] In temperate alpine areas with high snow accumulations, characteristic ablation features known as suncups form spontaneously on the snow during the spring and summer melting season [*Post and LaChapelle*, 2000]. It is likely that these intriguing patterns reduce the albedo of the snow and thereby increase the ablation rate through increased absorption of solar radiation. It has also been found that surface topography can significantly influence the interaction of wind with the snowpack with implications for energy transfer [*Smeets and van den Broeke*, 2008]. In an era of shrinking temperate glaciers, it is of interest to understand the factors that control the melt rate of snow since snowmelt is an important source for many of the world's rivers, which supply water for drinking, industry, and agriculture. Also, understanding this type of spontaneous pattern formation is an interesting problem in its own right with broader applications. For example, qualitatively similar patterns are observed in other ablation processes such as on the surface of meteorites (regmaglypts) [*Lin and Qun*, 1987] and in ion erosion of sputtering targets [*Munoz-Garcia et al.*, 2006].

[3] The surface morphology of snow has been explored from a variety of different perspectives. *Manes et al.* [2008] studied the scaling behavior of the surface roughness of fresh snow. The fractal dimension of the snow surface and surface roughness on multiple length scales have been measured by *Fassnacht et al.* [2009] for fresh snow at various times after snowfall. Suncups on the other hand, are an ablation phenomenon with a characteristic length that occurs on old snow. They have been investigated through field observations [*Rhodes et al.*, 1987], laboratory experiments [*Bergeron et al.*, 2006], and theoretical methods [*Betterton*, 2001; *Tiedje et al.*, 2006]. In this paper, we explore the growth and fluctuation of suncups with time-lapse observations and compare these observations with a mathematical model for suncups based on a nonlinear partial differential equation model developed earlier [*Tiedje et al.*, 2006].

[4] Our focus is on suncups on temperate snowfields at midlatitudes in which radiation-driven melting through direct exposure to the sun is the dominant ablation process. We do not address the more extreme snow surface ablation morphology known as penitentes. These occur at high elevations near the equator under rather different conditions where the humidity is low and sublimation is important [*Bergeron et al.*, 2006]. We also neglect the effect of turbulent heat transfer from the atmosphere, which is of secondary importance to radiative heat transfer during the melting process at our field sites [*Gray and Male*, 1981; *U.S. Army Corps Engineers*, 1956] and is outside the scope of our model.

[5] In earlier work, a model for suncups was developed in which the surface patterns are described by the solution of a nonlinear partial differential equation [*Tiedje et al.*, 2006]. This equation is similar to the Kuramoto-Sivashinsky equation used in fluid mechanics and in the theory of chemical reactions [*Sivashinsky and Michelson*, 1980; *Kuramoto and Tsuzuki*, 1975]. In earlier analysis described by *Tiedje et al.* [2006] a flat snow surface was found to be unstable against the formation of hollows due to the tendency for solar radiation to be concentrated at the bottom of concave regions on the surface. It was also found that the characteristic lateral size of suncups is related to the spectrally averaged diffusion length of solar radiation in snow. Numerical solutions of the nonlinear partial differential equation presented in this paper show that the surface patterns fluctuate chaotically in time. To see if suncups also fluctuate and to further refine the parameters in the mathe-

[1]Department of Mathematics, Simon Fraser University, Burnaby, British Columbia, Canada.
[2]Department of Electrical and Computer Engineering, University of Victoria, Victoria, British Columbia, Canada.

0148-0227/10/2010JF001724

matical model, we made time-lapse observations of suncups in the field.

2. Field Observation Sites

[6] Two field sites in southern British Columbia were used to explore the dynamics of suncups. The first site, at an elevation of 2240 m in the Selkirk Mountains (51°3′52″N, 117°32′0″W) was used to observe the initial formation of suncups. The Selkirk site is a generally level valley above the tree line and was partially covered with snow at the time of the observations (24–30 July 2007). The sky was clear for the entire 5 day period of the observations with the exception of a few hours one afternoon during which there were scattered clouds. As a result the snow was exposed to direct sun during the daytime for substantially the entire period of the observations.

[7] In order to investigate fluctuations in the suncup patterns, a second field site was established at an elevation of 2160 m near the summit of Whistler Mountain at 50°3′36″N, 122°57′38″W. The advantage of the Whistler site is that it has a pre-existing wireless infrastructure designed to service a downhill ski area. A webcam was mounted on a mast from which we were able to watch a snow bank several meters deep from an oblique angle during the period 21 July to 10 September 2007. The underlying rock started to become exposed 37 days into the observations on 29 August. The useful observations came to an end after 48 days on 10 September. By this time, the remaining snow surface area within the camera's view was a little less than half of what it had been prior to the exposure of the rock surface. The weather during the observations was mixed, with sun, cloud, some rain, and, on one occasion, a dusting of fresh snow.

[8] Meteorological data from weather stations nearby to both aforementioned sites are included in Appendix A.

3. Field Observations of Suncup Development

[9] The Selkirk observation site was used to observe the initial formation of suncups from an initially flat surface. The snow ablation rate was also measured at the Selkirk site with reference to a large rock which protruded through the snow about 10 m from the area of observation. The daily snow loss was measured by extrapolating the snow surface height to a point on a nearby rock surface (in an area where the snow was not shaded by the rock). The ablation rate of undisturbed suncup-covered snow was found to be 4.5 cm d^{-1}.

[10] We constructed two test patches 2–3.5 m in diameter in an approximately horizontal area by scraping off the surface layer with a shovel to flatten the snow surface, which lowered the snow surface relative to the surrounding area. At the end of the 5 day observation period, the suncups that had reformed on the flattened areas were indistinguishable visually from the suncups on untouched areas except that the snow loss was ~10 cm less and the snow was noticeably cleaner (compare snow surface with trench side wall in Figure 1a). This suggests that removing suncups and/or dirt increases the albedo, as one might expect.

[11] We investigated the snow surface using the standard technique of cross-sectional observation [*Manes et al.*, 2008; *Fassnacht et al.*, 2009]. Trenches 30 cm wide and 30 cm deep were cut with a shovel through the test patches as well as in an undisturbed area of snow in order to obtain cross-sectional images of the suncups. The trenches were cut at the end of the observation period without running into the ground at the bottom of the trench. This means the snow was at least 30 cm deep during the Selkirk site observations. According to *Gray and Male* [1982] as well as the *U.S. Army Corps Engineers* [1956], the optical thickness of snow is 10–30 cm. Radiation absorption by the underlying ground can therefore be neglected. All of the trenches were cut in a N-S direction and photographed at the same time (early in the morning when the sun was at oblique incidence) in order to give the best contrast.

[12] The trench edges were then manually digitized using photograph-editing software. A 60 cm ice axe and the 30 cm trench width were used as references to determine the angle of the snow surface relative to the camera's plane of view as well as its distance from the center of perspective [*Carlbom and Paciorek*, 1978]. From these parameters, we were able to infer the position of the digitized trench edges in three dimensions by performing an inverse perspective transformation. The forward perspective transform converts positions in space to pixel positions in the photographed image, while the inverse perspective transform undoes this operation [*Carlbom and Paciorek*, 1978]. This procedure yielded quantitative vertical height profiles and revealed that one camera pixel corresponded to a cross-sectional area in the range 1 × 1 mm to 2 × 2 mm. One of the photographs with digitized trench edges and a superimposed grid pattern indicating the inferred three-dimensional spatial information is shown in Figure 1a.

[13] The areas that were cross-sectioned represent three different stages of suncup development based on the time between when the snow was flattened and when the trenches were cut. Examples of transformed cross sections from each stage are shown in Figure 1. Two days after the surface has been flattened (Figure 1b), the dominant surface fluctuations are on a horizontal scale of 50–100 cm and appear approximately symmetric to vertical reflection. Five days after flattening (Figure 1c), the amplitude of these fluctuations has increased and is no longer reflection symmetric due to the formation of inverted V-shaped ridges. Finally, the cross section of the undisturbed region on which suncups have been allowed to develop for much longer than 5 days appears not to have further increased in amplitude relative to the 5 day cross section and possesses the same asymmetric topography. We therefore conclude that the surface amplitude has saturated after 5 days of ablation. The coincidence of this saturation with the appearance of asymmetric topography is consistent with the model discussed below. Similar measurements of snow cross sections in northern Colorado were made by *Fassnacht et al.* [2009], who observed that snow surface roughness increased during the melting process due partly to localized melt patterns.

[14] The one dimensional (1D) cross-sections were analyzed by finding the difference in height between adjacent local minima and maxima. The mean of these differences in the 5 day and undisturbed cross sections was found to be $h_c = 3.9 \pm 0.8$ cm. Since the cross sections do not typically pass through the lowest or highest point on the suncups, the heights obtained from cross sections will be smaller than the height of the full two-dimensional (2D) pattern. From

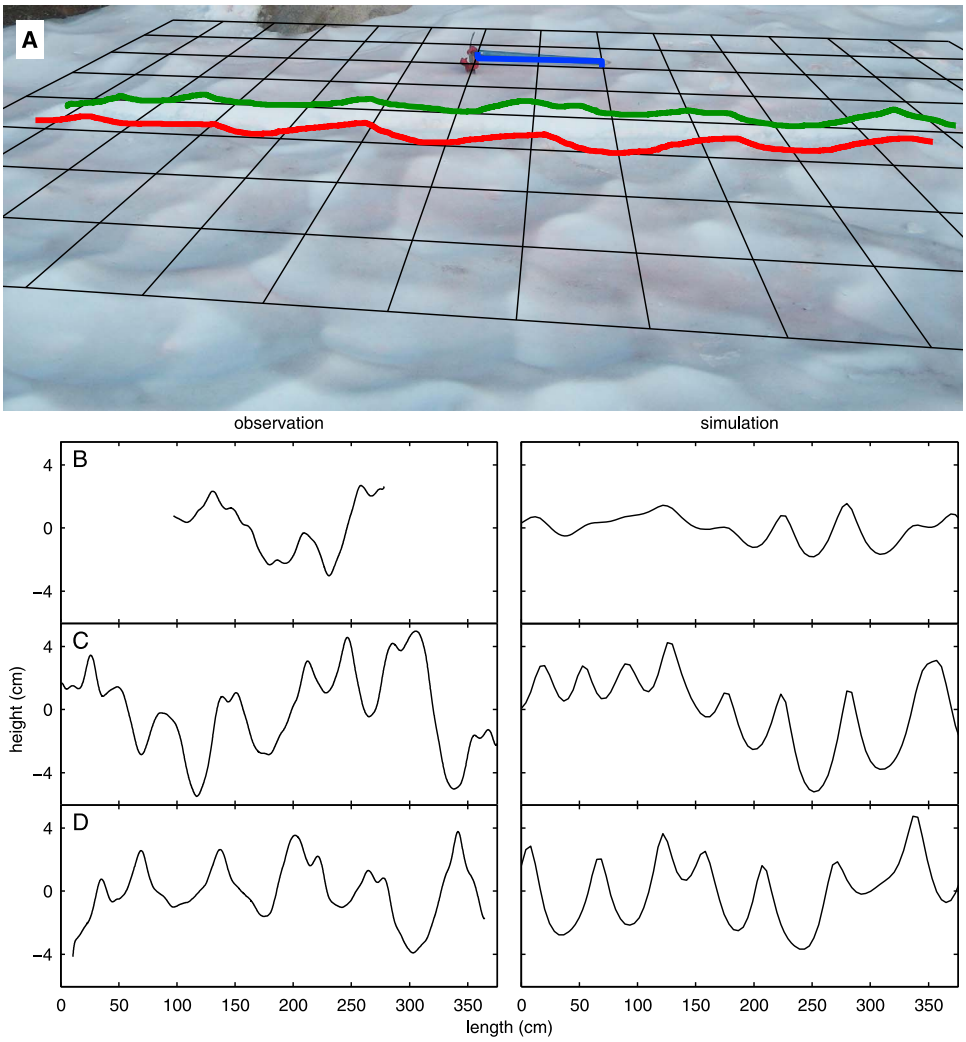

Figure 1. (a) Image of a N-S cross-section trench in an otherwise undisturbed area of snow with north to the right. The trenches were about 30 cm deep. The grid shown is oriented by eye and scaled to 30 cm grid spacing using the 60 cm ice axe and 30 cm wide trench as references. The edge of the snow surface is traced and projected onto a vertical plane using the resulting coordinate system as described in the text. The cross sections for three stages of suncup development are shown to the left of their appropriately scaled simulated counterparts for (b) 2 days after flattening, (c) 5 days after flattening, and (d) an undisturbed area. A single pixel in the original photograph corresponds to cross-sectional areas of approximately 1 × 1 mm to 2 × 2 mm in the "observation" column of Figures 1b–1d. The simulated cross sections are all integrated from the same random initial conditions.

the numerical simulations discussed below, the adjacent peak-to-valley height in the full 2D pattern is estimated to be larger than that observed in 1D cross sections by a factor of 1.5 ± 0.08. We therefore estimate that the full 2D height of the suncups after saturation is h_c = 5.6 ± 1.3 cm.

[15] The time dependence of the suncup height during their initial development was inferred from daily (morning and evening) visual observations and from the more accurate cross-sectional measurements as discussed above. The initial condition of the test patterns consisted of an area of snow that was flattened. By visual inspection, we estimate the initial 2D amplitude of the flattened areas on a 10–100 cm horizontal length scale to be about 1 cm. Further visual inspection measurements were also made after 1, 3, and 4 days while cross-sectional measurements were taken after 2 and 5 days, as well as in an undisturbed area. The visual observations considered the full 2D surface amplitude, while the cross sections considered only the amplitude of 1D surface profiles. Due to considerations discussed above, this is the predominant reason that the surface amplitudes obtained by visual inspection were found to be larger than those obtained from the cross sections by a factor of 1.7. The visual inspection measurements were therefore normalized by this factor. The estimated accuracy of the height measured by visual inspection was 20%. The heights measured from the cross section and by visual inspection are shown Figure 2. These data show that under the conditions at our observation site (full sun) the suncups are fully developed after 5 days, starting from a flat initial condition.

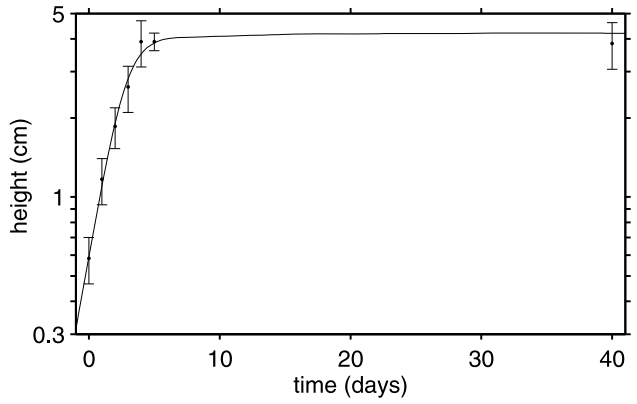

Figure 2. Growth in cross-sectional local peak to peak amplitude of snow surface topography both experimentally (points) and numerically for a value of $\theta = 0.7\pi$ (solid line). The first point is the estimated roughness of the starting surface, after being flattened with a shovel. The third, sixth, and last points are measured from digitized cross sections. The last point is taken from a cross section of an undisturbed area on the snow surface and its time is arbitrary except that its horizontal placement does not significantly affect the fit to the numerical data. The remaining points were obtained from visual observations of 2D surface amplitude and are therefore normalized to the cross-sectional measurements by dividing them by a factor of 1.7 as discussed in the text.

[16] The horizontal length scale of the cross sections was determined from their power spectral density. The cross sections were multiplied by a Hann window and zero-padded so that they were all the same length [*Press et al.*, 1992]. The modulus square of the fast Fourier transform (FFT) of the resulting profiles was computed and the spectra for cross sections in the same photograph were averaged together to improve statistical significance. To determine the characteristic length, the mean spectra were multiplied by wave number to remove low frequency noise and the location of the largest peak representing the characteristic length was found. In this way, the diameter of a suncup was estimated to be $l_c = 57 \pm 5$ cm. Similar dimensions (0.4–0.6 m) have been reported earlier for suncups in the Colorado Rockies by *Herzfeld et al.* [2003].

4. Field Observations of Suncup Dynamics

[17] The Whistler site was used to observe the dynamics of suncups after they had formed. During the period of observation, images were downloaded automatically from the site's webcam every minute. Digital images ranging in time from late afternoon to sunset were selected from each day for optimal contrast on the snow surface. The pixel positions in the images of the minima of 455 individual suncups were manually digitized for their observable lifetimes using a computer mouse to select their locations in each image. The positions of the minima were assumed to be located in the center of the suncups as defined by the surrounding ridges. The suncup minima are indicated in Figure 3b by black dots, while their trajectories deduced from previous images are shown by red tracks. During the first few days of observation, a 3.05 × 3.05 m square area was marked off by a rope on the snow surface. The area's vertices served as reference points for determining the parameters required to perform perspective transformations similar to those applied to the cross sections from the Selkirk site as discussed above.

[18] The photographic image is transformed to snow surface coordinates by first constructing a regular rectangular grid of points which correspond to the desired pixels in the transformed image. A forward perspective transform is used to project these points onto their corresponding pixel positions in the originally photographed image. Bicubic spline interpolation is used to compute the red, green and blue pixel values in the original image where these perspective-transformed points fall. The resulting array of interpolated pixels can then be assembled to yield an image of the surface as if it were viewed from directly above. Similarly, the locations of the digitized suncup minima in the original image are also transformed and superimposed onto this birds-eye-view image.

[19] Since we are concerned with the suncup dynamics relative to the mean surface motion, it is desirable to have the transformed image coordinates follow the overall surface motion as it recedes with melting. Therefore, the parameters of the perspective transformation were adjusted for each day using a simplex optimization routine [*Lagarias et al.*, 1998] that minimized the mean square distance traveled by all the suncup minima between consecutive days. Since the number of points tracked is large, fluctuations of individual minima are averaged out to yield transform parameters that track the total mean surface movement to a very good approximation.

[20] The horizontal location on the surface is measured in units of characteristic lengths. The characteristic length is determined by taking the peak of the radially averaged power spectral density of the birds-eye-view snow surface image averaged over the period of observation. This power spectral density is obtained using similar methods to those described for the surface cross sections from the Selkirk site, except that the FFT is taken in two dimensions and the resulting 2D power spectral density is averaged around circles of constant wave number magnitude in Fourier space. Upon transforming and scaling the images in this way, it is found that a single pixel as sampled by the site's webcam in the original image corresponds to a snow surface area ranging from 0.02 × 0.02 to 0.08 × 0.08 unitless characteristic lengths.

[21] The measured root-mean-square (RMS) displacement of the digitized and transformed suncup minima is plotted as a function of time in Figure 4. A correction for the systematic measurement error as well as the calculation of the error bars is discussed in Appendix B. The motion of the suncups is consistent with diffusion, in that the displacement increases with the square root of time. The 1 day diffusion length, is defined as the RMS displacement after 1 day averaged over all the suncups. In this way, we estimate a diffusion length of 0.07 ± 0.01 characteristic lengths, or equivalently $0.07 \times 57 = 4.1 \pm 0.5$ cm using 57 cm as the characteristic spacing of the suncups. From this, we estimate the diffusion coefficient of the suncups to be $D = 4.1^2 / 2 = 8.3 \pm 2$ cm^2 d^{-1}. Expressed in a different way, this means

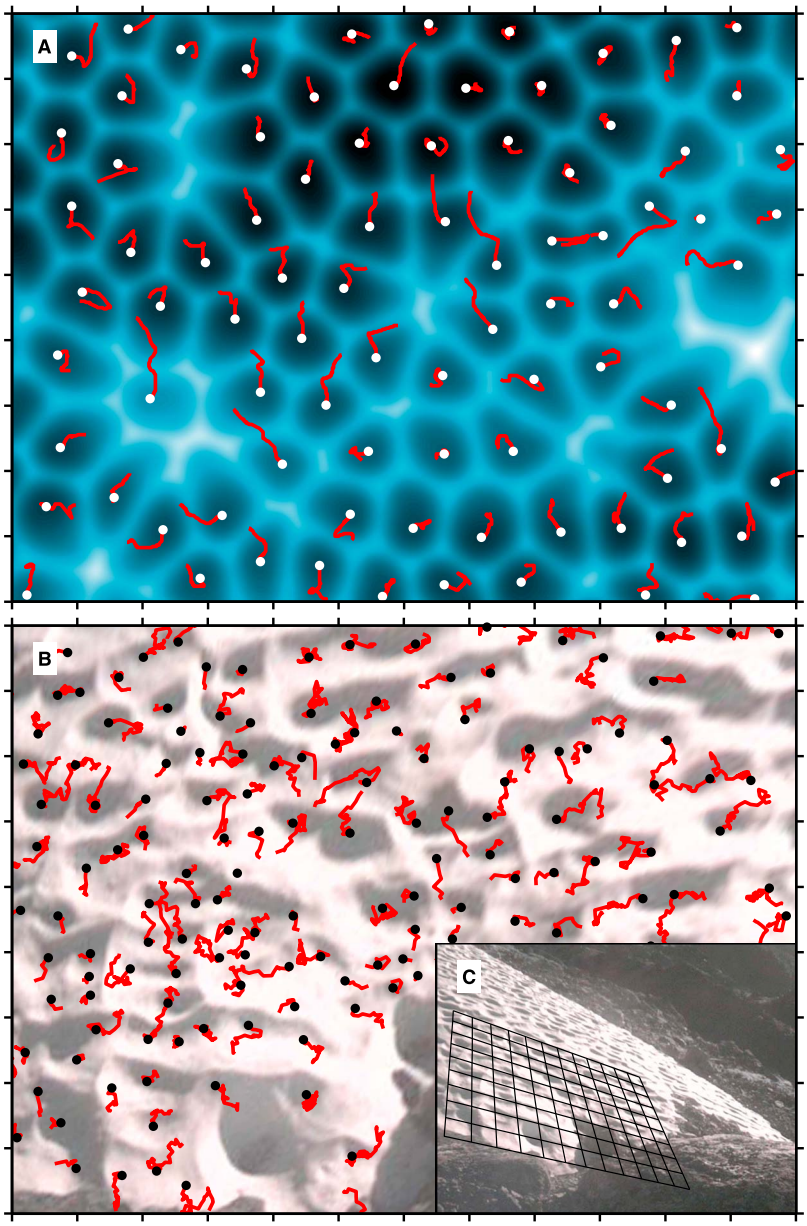

Figure 3. Trajectories of suncup minima in (a) numerical simulation at $\theta = 0.7\pi$ and (b) field observations at the Whistler site. Dots correspond to the location of the minima in the images shown, while red lines show the trajectory of the minima as inferred from previous images. Outer tick mark spacing is equal to the measured horizontal characteristic length of the surface. (c) The original image from which the transformed surface in Figure 3b was derived, with grid lines corresponding to tick marks in the transformed image. A single pixel in the original image corresponds to a snow surface area ranging between 0.02 × 0.02 and 0.08 × 0.08 unitless characteristic lengths in the transformed image.

that in 30 days an individual suncup will diffuse 22 cm on average, or less than half of a typical suncup diameter.

5. Nonlinear Partial Differential Equation Model

[22] Earlier work has shown that solutions of the following partial differential equation reproduce a number of the salient features of suncups [*Tiedje et al.*, 2006]:

$$\frac{dh}{dt} = -F - c_1\nabla^2 h - c_2\nabla^4 h + c_3|\nabla h|^2 + c_4\nabla^2|\nabla h|^2. \quad (1)$$

In this equation, $h(x, y, t)$ is the surface height as a function of horizontal position and time measured with respect to a reference plane. At $t = 0$, the surface is assumed to be nearly flat with a small random topography. The F is the ablation rate of a flat snow surface. In order to spontaneously form the suncup pattern, coefficients c_1 and c_2, must both be positive. In this case, the first linear term (∇^2) is unstable and dominant at long wavelengths while the second linear term (∇^4) is stable and dominant at short wavelengths. The most unstable wavelength defines a characteristic length scale for individual suncups. The signs of the nonlinear

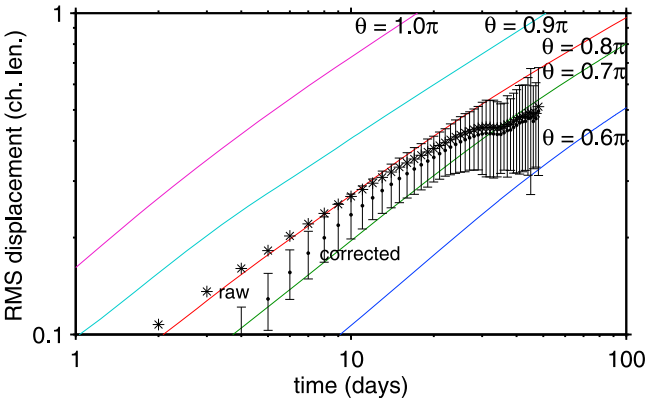

Figure 4. Root-mean-square (RMS) displacement of the minima of simulated suncups and suncups observed at the Whistler site. Displacement is shown in units of characteristic lengths for purposes of comparison. For reference the characteristic length measured at the Selkirk site was $l_c = 57 \pm 5$ cm. Both the raw data and data corrected for systematic error are shown. The procedure by which this systematic correction is carried out as well as the computation of the error bars is discussed in Appendix B.

coefficients c_3 and c_4 define the characteristic shape of the solution. The shape of the suncups, with their characteristic rounded bottoms and inverted V-shaped ridges, requires that c_3 be negative and c_4 be positive. The physical origin of these terms is discussed by *Tiedje et al.* [2006].

[23] It is noteworthy that all of the terms in equation (1) are conservative with the exception of the flat surface ablation rate F and the first nonlinear term $c_3|\nabla h|^2$. By conservative, we mean that the average of the term over the surface is zero; therefore, it has no net effect on the global ablation rate on average. Since $|\nabla h|^2$ is always positive, it cannot have this property. When c_3 is negative, this nonconservative term acts to increase the net ablation rate from that of the flat surface. If ablation is due to the absorption of solar radiation by the snow, then a measurement of $c_3|\nabla h|^2$ tells us the effect of the suncups on the spectrally integrated albedo. In the context of the observed shape of suncups (rounded valleys, inverted V-shaped ridges), equation (1) tells us that the albedo of snow must decrease when the suncup pattern forms.

[24] We can convert (1) to a dimensionless form by substituting $\hat{t} = t/t_0$, $\hat{h} = h/h_0$, and $\hat{x} = xq_0$ where the characteristic time, height, and spatial frequency are given by $t_0 = c_2/c_1^2$, $h_0 = 1/\sqrt{(c_3/c_1)^2+(c_4/c_2)^2}$, and $q_0 = \sqrt{c_1/c_2}$, respectively. With these substitutions the equation can be written in the dimensionless form

$$\frac{d\hat{h}}{d\hat{t}} = -\hat{F} - \hat{\nabla}^2\hat{h} - \hat{\nabla}^4\hat{h} + \cos\theta\left|\hat{\nabla}\hat{h}\right|^2 + \sin\theta\hat{\nabla}^2\left|\hat{\nabla}\hat{h}\right|^2, \qquad (2)$$

where $\hat{F} = Ft_0/h_0$ is the dimensionless ablation rate and $\cos\theta = h_0c_3/c_1$ is a free parameter. The sine and cosine constrain the sum of squares of the nonlinear coefficients to be equal to unity so that only their ratio can vary. We restrict $\theta \in [\pi/2, \pi]$ so that the signs of the nonlinear terms are consistent with the shape of suncups as discussed above.

[25] In an earlier paper [*Tiedje et al.*, 2006], we showed that numerical solutions of equation (1) share a number of common features with suncups: A quasi-periodic pattern with a characteristic length, rounded valleys separated by inverted V-shaped ridges, and a surface height that grows exponentially from low amplitude initial conditions until it saturates at a characteristic height that is independent of the particular initial conditions used. Theoretical values were obtained for the characteristic length, height, and growth time based on an approximate treatment of the absorption of solar radiation in snow derived from its known optical properties. Although the theoretical model for the coefficients of the linear terms gives values for the characteristic length that are in reasonable agreement with observations, the model predicts the wrong sign for c_3, the coefficient of the first nonlinear term. In the earlier work, the dynamical behavior of the suncup patterns after the height had saturated was not explored [*Tiedje et al.*, 2006]. This is a topic of particular interest for the present paper as we explain below.

[26] Given an initial surface height consisting of low amplitude white noise, solutions to equation (1) exhibit long wavelength surface fluctuations that grow exponentially in time. The characteristic length of the fastest growing fluctuations is $l_c = 2\pi\sqrt{2}/q_0$. Eventually these modes dominate the solution, and a quasi-periodic pattern is formed. According to a solution of the linear part of the equation at the characteristic length, the characteristic time for the exponential growth is $t_c = 4t_0$. Numerical solutions show that the topography increases until the local peak-to-peak amplitude reaches a characteristic height $h_c \sim 4\ h_0$, at which point, it remains relatively constant. As with the observational data, the appearance of the inverted V-shaped ridges in the model is coincident with the height saturation as shown in Figures 1b–1d.

[27] Once the surface height saturates, the surface pattern may fluctuate in time since (1) is a nonlinear equation, with possibly chaotic solutions. In order to explore the temporal behavior of the patterns, numerical solutions of equation (2) were carried out. Two different size square periodic domains, with sides of dimensionless lengths of 32π and 64π were employed to ensure the results are independent of the size of the simulated surface. Spatial differentiation was done in the Fourier domain and a fourth-order Runge-Kutta exponential time-differencing method was used to advance the solution in time [*Kassam and Trefethen*, 2005]. This method has the advantage of integrating the stiff linear terms exactly.

[28] To facilitate comparison with observations of real suncups, we find the dimensional timescale t_0 for each θ simulated by performing a fit to the exponential growth data, similar to that shown in Figure 2. Uncertainty in the resulting fit parameters is computed by taking the standard deviation of a set of 10,000 such parameters, each computed by performing the fit with the observational data points perturbed by normally distributed independent random numbers with standard deviations equal to the data point uncertainty as indicated by the error bars in Figure 2. Additionally, the length scale is measured in units of the characteristic length, determined for each θ from the peak in the time-averaged radial power spectral density of the fully height-saturated solution. The radial power spectral density is computed in the same way as for the snow surface image

described above, except that no zero-padding or windowing is necessary since the simulated surface is naturally periodic. The measurement of characteristic length and time-scale for each θ is necessary as they depend weakly on θ in the range considered.

[29] The numerical solutions show that the surface pattern does indeed fluctuate chaotically once the amplitude of the pattern saturates. In addition, we find that the rate of the fluctuations increases for increasing values of θ in equation (2). To quantify the speed of the fluctuations, we track the positions of the minima as a function of time in the simulated patterns as shown in Figure 3a. Averaging the square of the displacements for all suncups, and plotting the RMS displacement as a function of time, we find that the displacement increases approximately with the square root of time as shown by the solid lines in Figure 4. This scaling of displacement as the square root of time is similar to ordinary diffusion. It is remarkable that the chaotic behavior of the solution of equation (1) can be characterized simply by the statement that the individual minima exhibit Brownian motion. Furthermore, the log of the RMS displacements in Figure 4 is approximately proportional to θ over the range considered. This means the diffusion constant for the individual suncups increases exponentially with θ. It follows that a measurement of the rate of diffusion for suncups can be used to infer θ and hence the size of the nonconservative coefficient in equation (1).

6. Discussion

[30] The model can be compared with the observations at two levels: First, whether the equation itself can describe the observations taking the coefficients in the equation to be free parameters; second, whether the coefficients in the equation are consistent with the predictions of the physical model based on solar radiation transport and absorption in snow.

[31] On the first point, the observed growth in the height of the suncups is consistent with the exponential increase followed by saturation predicted in the model as shown in Figure 2. In Figure 2, the coefficients in the equation are treated as fitting parameters. The characteristic time in the exponential growth phase obtained from the fit is $t_c = 1.5 \pm 0.3$ days. This is significantly shorter than the 9 days predicted theoretically from the radiation transport and absorption model [*Tiedje et al.*, 2006].

[32] Predicted values for l_c and h_c, the characteristic length and height, have also been obtained earlier from the optical absorption and scattering properties of snow [*Tiedje et al.*, 2006; *Wiscombe and Warren*, 1981]. The observed characteristic size of the suncups matches the theoretical value (also 57 cm; exact match is a coincidence) obtained earlier from the optical properties of snow [*Tiedje et al.*, 2006]. The measured amplitude (5.6 cm) is an order of magnitude smaller than the theoretical value (59 cm), although much deeper suncups have been reported in other locations [*Post and LaChapelle*, 2000]. The height scale h_0, as defined above, depends on the nonlinear terms, whereas the length scale l_0 depends only on the linear terms. It is not surprising that there is a large discrepancy in the amplitude of the suncups but not in their lateral size, since the coefficients of the nonlinear terms are not well understood theoretically.

[33] By comparing the diffusion of the real suncups with the simulations in Figure 3, we find that the observations match the numerical results best for $\theta = (0.73 \pm 0.1)\pi$, as shown in Figure 4. We can estimate the coefficient of the first nonlinear term in the differential equation from the value of θ. As discussed above, this term is of interest because it is the only nonconservative term in the equation and therefore the only term which affects the melt rate and consequently the albedo. The nonconservative term increases the ablation rate by the amount

$$\Delta F = c_3 \left\langle |\nabla h|^2 \right\rangle = \cos\theta \frac{h_0}{t_0} \left\langle \left|\hat{\nabla}\hat{h}\right|^2 \right\rangle = 1.7 \ \pm \ 0.4 \text{ cm d}^{-1}, \tag{3}$$

where the average $\langle |\hat{\nabla}\hat{h}|^2 \rangle = 0.5 \pm 0.1$ is computed from the numerical model of the surface with θ as estimated above. As discussed above, the total ablation rate including the effect of the suncups and surface contaminants is $F + \Delta F = 4.5$ cm d^{-1}, so that the fractional increase in ablation rate is $\Delta F/F = 0.6 \pm 0.3$. If snow ablation is dominated by solar radiation input then faster snow ablation means more radiation is absorbed and therefore the intensity of the reflected radiation (and the albedo) is reduced. This analysis neglects the secondary role played by turbulent heat flux in the atmosphere. It also rests on the assumption that the snowpacks observed were optically thick so that the albedo of the underlying surface is not significant. This assumption certainly holds for the Selkirk site. It also holds for the Whistler site up to a few days before the exposure of the rock surface, given the ablation rate of 4.5 cm d^{-1}. The inferred increase in ablation rate represents a surprisingly large reduction in albedo, although the uncertainty is large.

[34] An independent measure of the change in albedo is available from the observation that there was ~10 cm less snow loss on the test patch 5 days after being flattened. This can be attributed to two effects: The reduced amplitude of suncups during this period and the absence of dirt on the freshly flattened snow, which was visibly whiter. If we assume that the change in albedo due to partially developed suncups is related to the ΔF of saturated suncups via the ratio of the squared height to the fully saturated squared height, then the additional loss on a given day is $\Delta F(h(t)/h(\infty))^2$. The cumulative effect after 5 days of suncup growth is then given by the integral $\int_0^5 \Delta F(h(t)/h(\infty))^2 \, dt = (2.4 \pm 0.5)\Delta F$ which is computed by numerically integrating the surface height in Figure 2. We also expect a change in albedo due to the dirt, ΔF_{dirt}, which is not affected by the surface topography and therefore has a 5 day cumulative effect given simply by $5\Delta F_{\text{dirt}}$. We can account for the reduced snow loss by these two effects:

$$10 \text{ cm} = 2.4\Delta F + 5\Delta F_{\text{dirt}}. \tag{4}$$

Solving for ΔF, we find that $\Delta F = 4.2$ cm d^{-1} $- 2.1\Delta F_{\text{dirt}}$. This is consistent with the above estimate of $\Delta F = 1.7$ cm d^{-1} if $\Delta F_{\text{dirt}} = 1.2$ cm d^{-1} and with *Rhodes et al.* [1987], who found that surface dirt can increase the ablation rate by up to 90%, almost doubling the ablation rate.

[35] Clearly the above analysis could benefit from more accurate measurements. A source of error that has not been fully accounted for is that associated with visually inferring

Table A1. Mean and Standard Deviation of Hourly Meteorological Data Collected From the Golden Airport Weather Station Between 24 and 30 July 2007[a]

	Mean	Standard Deviation
Temperature (°C)	21.0	6.6
Dew Point (°C)	9.3	2.4
Relative Humidity (%)	53	23
Wind Direction (°)	150	140
Wind Speed (km/h)	8	8
Visibility (km)	48	4
Pressure (kPa)	92.31	0.29

[a]Data from http://climate.weatheroffice.gc.ca/climateData/canada_e.html. Data were only available between 0500 and 1800 LST, but were otherwise consistent. The station was approximately 50 km east of and 1460 m lower in elevation than the Selkirk observation site.

Table A2. Mean and Standard Deviation of Hourly Meteorological Data Collected From the Revelstoke Airport Weather Station Between 24 and 30 July 2007[a]

Reported	Mean	Standard Deviation
Temperature (°C)	21.2	6.0
Dew Point (°C)	10.4	2.6
Relative Humidity (%)	56	24
Wind Direction (°)	200	140
Wind Speed (km/h)	10	8
Visibility (km)	15	0
Station Pressure (kPa)	96.02	0.27

[a]Data from http://climate.weatheroffice.gc.ca/climateData/canada_e.html. Five hourly reports on 26 July did not contain all variables and are not included in the calculation. This station was approximately 50 km to the west of and 1795 m lower in elevation than the Selkirk observation site.

the position of the suncup minima. A laser profilometer with an accuracy of 1 mm viewing a large field of suncups from a position high overhead such as on a ski lift tower would directly measure the surface topography giving more accurate and objective positions for the minima. Such an experiment would have a much smaller error in the measurement of the suncup positions and therefore reduce the importance of estimating and subtracting the systematic error as discussed in Appendix B.

7. Conclusion

[36] In conclusion, we have compared field observations of the size and dynamics of suncups in a temperate alpine area with a numerical model based on a nonlinear partial differential equation. Although the model itself was proposed earlier, the analysis of the model has been extended to include an investigation of the dynamics of the characteristic patterns that are produced. The model is in excellent agreement with observations, if we treat the four coefficients in the equation as adjustable parameters. The observed characteristic lateral size of the suncups matches the predictions of a model based on solar radiation transport and absorption in snow; however, the growth rate and depth of the suncups do not. Under full sun, suncups were found to develop to their saturation height in about 5 days. Individual suncups are observed to move randomly over time, with a diffusive motion, mimicking the chaotic fluctuations observed in the model. The nonlinear partial differential equation predicts that the rate of lateral diffusion of the suncups can be used to infer the reduction in the albedo caused by the suncups. Conversely, this relationship suggests that direct albedo measurements might give useful information about the morphology of the snow surface. More accurate measurements of the diffusive motion of suncups as well as direct measurements of their albedo are needed to better understand the relation between these two phenomena.

Appendix A: Meteorological Observations

[37] Several Environment Canada weather stations were used to obtain meteorological information during the time of observations. The data from these stations is accessible online from Canada's National Climate Data and Information Archive (available at http://climate.weatheroffice.gc.ca/climateData/canada_e.html).

[38] The two nearest meteorological stations to the Selkirk site that were operating during the observation period are approximately 50 km to the east or west and about 1500 m lower in elevation than the Selkirk site. The Golden Airport weather station to the east (51°17′54.000″N, 116°58′54.000″W) was at an elevation of 785 m and reported hourly each day between 0500 and 1800 local standard time (LST) the temperature, dew point temperature, relative humidity, wind speed, and direction, visibility, station pressure, and qualitative atmospheric conditions. Throughout the duration of the Selkirk observations, 84 hourly atmospheric observations were taken during observed daylight hours (0600–1800 LST). Of these, 22 reported "Clear," 44 reported "Mainly Clear," and 18 reported "Mostly Cloudy." The quantitative data from the Golden Airport station are summarized in Table A1.

[39] The Revelstoke Airport weather station to the west of the Selkirk site (50°57′40.00″N, 118°11′0.00″W) was at an elevation of 445 m. This station reported the same variables as the Golden Airport station; however, it reported hourly 24 hours a day with the exception of 5 hours on 26 July 2007 in which some of the variables were not reported. Its atmospheric condition reports were more sparse. There were 112 total daylight hours during the Selkirk observations. During these hours, the Revelstoke Airport's log of atmospheric observations reported 1 hour of "Drizzle" while all other daylight hours had an entry of either nothing or "NA." The quantitative data from the Revelstoke Airport station are summarized in Table A2.

Table A3. Mean and Standard Deviation of Hourly Meteorological Data Collected From the Whistler Mountain High Level Weather Station Between 24 July and 10 September 2007[a]

Reported	Mean	Standard Deviation
Temperature (°C)	8.9	3.8
Dew Point (°C)	4.3	2.2
Relative Humidity (%)	76	17
Station Pressure (kPa)	83.59	0.32

[a]Data from http://climate.weatheroffice.gc.ca/climateData/canada_e.html. Seven nonconsecutive hourly data points were missing and are not included in the calculation. This station was approximately 2 km to the northeast of and 520 m lower in elevation than the Whistler webcam site.

Table A4. Mean and Standard Deviation of Hourly Meteorological Data Collected From the Whistler Mountain High Level Remote Wind Weather Station Between 24 July and 10 September 2007[a]

	Mean	Standard Deviation
Temperature (°C)	9.3	3.9
Wind Direction (°)	200	90
Wind Speed (km/h):	8	5

[a]Data from http://climate.weatheroffice.gc.ca/climateData/canada_e.html. Data for all hours in this time span were consistently available. This station was approximately 2 km to the northeast of and 470 m lower in elevation than the Whistler webcam site.

[40] There were two monitoring stations approximately 2 km northeast of and 500 m below the elevation of the Whistler site. The Whistler Mountain High Level station (50°04′37.034″N, 122°56′46.050″W) was at an elevation of 1640 m and reported hourly temperature, dew point, relative humidity, and station pressure. The Whistler Mountain High Level Remote Wind station (50°04′27.030″N, 122°56′49.000″W) at an elevation of 1690 m also reported hourly temperature in addition to wind speed and direction. There were no qualitative atmospheric observations from either of these sites. The quantitative observations are summarized in Tables A3 and A4.

Appendix B: Error Analysis of Observational Trajectories

[41] We quantify the error associated with manually digitizing the suncups by redigitizing a sample of 20 suncup trajectories and computing the squared difference $|\delta\vec{x}|^2$ between the resulting minima locations and those originally digitized. If we consider each such measurement drawn from a two-dimensional (2D) normal distribution centered at the true suncup position with standard deviation σ in each direction, then the expectation of these discrepancies is $4\sigma^2$, from which we find that $\sigma = \sqrt{\left\langle \left|\delta\vec{x}\right|^2 \right\rangle} \Big/ 2 = 0.06$ characteristic lengths.

[42] The result is that we can say that our measurement of the position of a given suncup $\vec{X}$ is the sum of the true position $\vec{x}$ and a random error $\sigma\vec{u}$ where $\vec{u}$ is a random vector with independent standard normal components,

$$\vec{X} = \vec{x} + \sigma\vec{u}\ . \tag{B1}$$

What we measure for Figure 4 is the squared change in $\vec{X}$ between two measurements:

$$\left|\Delta\vec{X}\right|^2 = \left|\Delta\vec{x} + \sigma\left(\vec{u}_b - \vec{u}_a\right)\right|^2. \tag{B2}$$

The subtraction of the two random vectors creates a new random vector $\vec{u}_b \cdot \vec{u}_a = \sqrt{2}\,\vec{u}_c$. We may then expand the square as

$$\left|\Delta\vec{X}\right|^2 = \left|\Delta\vec{x}\right|^2 + 2\sigma^2\left|\vec{u}_c\right|^2 + 2\sqrt{2}\sigma\left|\Delta\vec{x}\right|u_d, \tag{B3}$$

where we have used the fact that since $\Delta\vec{x}$ and $\vec{u}$ are independent, their dot product is a new scalar random variable $\Delta\vec{x} \cdot \vec{u}_c = |\Delta\vec{x}|u_d$. Since $\vec{u}_c$ and u_d are standard normal random variables, we find that $\langle|\vec{u}_c|^2\rangle = 2$ and $\langle u_d\rangle = 0$. Consequently, taking the average over equation (B3), we find that we must subtract $4\sigma^2$ from our measured mean square distances to obtain the true mean square distance

$$\left\langle \left|\Delta\vec{x}\right|^2 \right\rangle = \left\langle \left|\Delta\vec{X}\right|^2 \right\rangle - 4\sigma^2. \tag{B4}$$

[43] The most significant source of random uncertainty is the approximation of the expectation $\langle|\Delta\vec{X}|^2\rangle$ by a finite sum. This is quantified by the standard error assuming that ΔX is a Gaussian. In fitting to the numerical data, we must also account for uncertainties in the time scale, which are associated with fitting the initial roughening data $\delta t_0/t_0 \approx 20\%$. We note that $\langle|\Delta\vec{x}(\Delta t)|^2\rangle \propto \Delta t$ since it is approximately Brownian and therefore the time-scale uncertainty contributes a relative error of $\delta t_0/t_0$ to $\langle|\Delta\vec{x}|^2\rangle$. To estimate the cumulative uncertainty in $\langle|\Delta\vec{x}|^2\rangle$, as shown by the error bars of Figure 4, we add the above contributions in quadrature.

[44] **Acknowledgments.** We thank Tom Green of Tranzeo Wireless, Kathy Jenkins of Whistler-Blackcomb, as well as Doug Brown and Sandra McGuinness of the Kootenay Mountaineering Club for their help with the field observations.

References

Bergeron, V., C. Berger, and M. D. Betterton (2006), Controlled irradiative formation of penitentes, *Phys. Rev. Lett.*, *96*, 098502, doi:10.1103/PhysRevLett.96.098502.

Betterton, M. D. (2001), Theory of structure formation in snowfields motivated by penitentes, suncups, and dirt cones, *Phys. Rev. E*, *63*, 056129, doi:10.1103/PhysRevE.63.056129.

Carlbom, I., and J. Paciorek (1978), Planar geometric projections and viewing transformations, *ACM Comput. Surv.*, *10*, 465–502.

Fassnacht, S. R., M. W. Williams, and M. V. Corrao (2009), Changes in the surface roughness of snow from millimeter to meter scales, *Ecol. Complexity*, *6*, 221–229, doi:10.1016/j.ecocom.2009.05.003.

Gray, D. M., and D. H. Male (1981), *Handbook of Snow: Principles, Processes, Management, and Use*, Pergamon, Willowdale, Ont., Can.

Herzfeld, U. C., H. Mayer, N. Caine, M. Losleben, and T. Erbrecht (2003), Morphogenesis of typical winter and summer snow surface patterns in a continental alpine environment, *Hydrol. Processes*, *17*, 619–649, doi:10.1002/hyp.1158.

Kassam, A. K., and L. N. Trefethen (2005), Fourth-order time-stepping for stiff PDE's, *SIAM J. Sci. Comp.*, *26*, 1214–1233, doi:10.1137/S1064827502410633.

Kuramoto, Y., and T. Tsuzuki (1975), Formation of dissipative structures in reaction-diffusion systems: Reductive perturbation approach, *Prog. Theor. Phys.*, *54*, 687–699, doi:10.1143/PTP.54.687.

Lagarias, J. C., J. A. Reeds, M. H. Wright, and P. E. Wright (1998), Convergence properties of the Nelder-Mead simplex method in low dimensions, *SIAM J. Optim.*, *9*, 112–147, doi:10.1137/S1052623496303470.

Lin, T. C., and P. Qun (1987), On the formation of regmaglypts on meteorites, *Fluid Dyn. Res.*, *1*, 191–199, doi:10.1016/0169-5983(87)90004-9.

Manes, C., M. Guala, H. Loewe, S. Barlett, L. Egli, and M. Lehning (2008), Statistical properties of fresh snow roughness, *Water Resour. Res.*, *44*, W11407, doi:10.1029/2007WR006689.

Munoz-Garcia, J., M. Castro, and R. Cuerno (2006), Nonlinear ripple dynamics on amorphous surfaces patterned by ion beam sputtering, *Phys. Rev. Lett.*, *96*, 086101, doi:10.1103/PhysRevLett.96.086101.

Post, A., and E. R. LaChapelle (2000), *Glacier Ice*, Revised Ed., Univ. Wash. Press, Seattle, Wash.

Press, W. H., S. A. Teukolsky, W. T. Vetterling, and B. P. Flannery (1992), *Numerical Recipes in Fortran: The Art of Scientific Computing*, 2nd Ed., Cambridge Univ. Press, New York.

Rhodes, J. J., R. L. Armstrong, and S. G. Warren (1987), Mode of formation of ablation hollows controlled by dirt content of snow, *J. Glaciol.*, *33*, 135–139.

Sivashinsky, G. I., and D. M. Michelson (1980), On irregular wavy flow of liquid-film down a vertical plane, *Prog. Theor. Phys.*, *63*, 2112–2114.

Smeets, C. J. P. P., and M. R. van den Broeke (2008), Temporal and spatial variations of the aerodynamic roughness length in the ablation zone of the Greenland ice sheet, *Boundary Layer Meteorol.*, *128*, 315–338, doi:10.1007/s10546-008-9291-0.

Tiedje, T., K. A. Mitchell, B. Lau, A. Ballestad, and E. Nodwell (2006), Radiation transport model for ablation hollows on snowfields, *J. Geophys. Res.*, *111*, F02015, doi:10.1029/2005JF000395.

U.S. Army Corps Engineers (1956), *Snow Hydrology*, U.S. Army Corps of Eng., North Pacific Div., Portland, Oreg.

Wiscombe, W. J., and S. G. Warren (1981) A model for the spectral albedo of snow, *J. Atmos. Sci.*, *37*, 2712–2733.

K. A. Mitchell, Department of Mathematics, Simon Fraser University, Burnaby, BC V6T 1Z4, Canada. (kevmitch@math.sfu.ca)

T. Tiedje, Department of Electrical and Computer Engineering, University of Victoria, Victoria, BC V8W 3P6, Canada.